Inverse quantum-mechanical control: A means for design and a test of intuition

Peter Gross, Harjinder Singh,* and Herschel Rabitz
Department of Chemistry, Princeton University, Princeton, New Jersey 08544

Kenneth Mease
Department of Mechanical and Aerospace Engineering, Princeton University, Princeton, New Jersey 08544

G. M. Huang
Department of Electrical Engineering, Texas A&M University, College Station, Texas 77843
(Received 28 September 1992)

The inverse quantum-mechanical control of molecules is studied using the equation of motion for the expectation value of an operator. With this method, a requisite external field is obtained to track exactly a prescribed molecular objective expectation value as a function of time. Applications to diatomic and polyatomic molecules are formulated. While the method is directly applicable as a test of physical intuition, it can in principle be used to design fields for specific objectives including reactive selectivity. Results are presented for position and energy tracking in the hydrogen fluoride molecular system. The numerical calculations show that seemingly benign objective tracks may give rise to singularities in the field. However, these singularities do not present problems in the evolution of the dynamical quantities and instead provide useful hints for designing robust fields.

PACS number(s): 03.65.−w, 31.15.+q

I. INTRODUCTION

Control of chemical dynamics using external laser fields has received considerable theoretical attention in recent years [1–4]. Generally, the problem is posed in terms of designing a field which will produce a specific physical goal in a molecular system, e.g., cleavage of a particular bond. To date, an especially attractive general approach to the problem has employed the optimal control theory [5], a mathematical tool commonly used in the engineering fields. In this method the relevant physical aspects of the problem are translated into a mathematical cost functional whose minimization with respect to the electric (control) field function aims to achieve a particular set of physical goals. The optimal control method is appealing because it allows for wide flexibility in choosing the relative importance of various desired objectives and penalties. A drawback is that even for mildly complex systems (including small molecules) the minimization of the objective functional must be performed by an often computationally intensive iterative optimization procedure.

In this work we explore an alternative method for designing fields which produce specified objectives in quantum-mechanical systems based on nonlinear inverse control theory [6]. The use of inverse control is conceptually simple and largely unexplored in molecular dynamics, although it has been used in robot and other engineering control problems. In simple terms, in the inverse control approach, the time-dependent path of a desired observable expectation value $\langle \hat{O} \rangle_t = y_d(t)$ is specified *a priori*, and one seeks the control optical field $E(t)$ that will *exactly* meet the demand. If the expectation value $y_d(t)$ is chosen reasonably, then desirable control will be achieved without resorting to an iterative optimization procedure. This procedure can, in fact, be shown to be equivalent to optimal tracking of an observable using the optimal control method where the cost functional contains nothing but the tracking demand. In this paper we present some applications and an evaluation of the inverse quantum-mechanical control approach.

The theoretical basis for the inverse quantum-mechanical control was established by Ong *et al.* [7,8], who developed necessary and sufficient conditions for the existence and uniqueness of the solution to the inverse quantum-mechanical control problem [7,8]. In this paper, we apply the inversion procedure to position and energy tracking in a diatomic system. The practical difficulties arising from possible singularities in the field obtained by inversion are also discussed.

We are also pursuing inverse control for an analogous classical mechanical problem [9] which has a connection to recent studies on classical goal dynamics tracking [10]. In this paper, we will confine ourselves to presenting results for quantum-mechanical inverse control only, but the procedure is completely analogous to that for the classical problem.

The balance of the paper is as follows. In Sec. II, we define the control model for a quantum-mechanical system and the inverse control approach. The connection to optimal control theory is also shown. Section III develops the application to different tracking problems and discusses the issues of singularities arising from the inverse control formulation. Results for the inverse quantum-mechanical position and energy tracking for a diatomic molecule are presented in Sec. IV. Concluding remarks and future perspectives are presented in Sec. V,

and a proposed method for application of the inverse control method to polyatomic systems is discussed in the Appendix.

II. THE CONTROL SYSTEM AND THE INVERSE PROBLEM

We consider here a molecular system interacting with an external field $\mathbf{E}(t)$. Its evolution is governed by Schrödinger's equation

$$i\hbar\frac{\partial\psi(\mathbf{r},t)}{\partial t}=[\hat{H}_0-\boldsymbol{\mu}(\hat{\mathbf{r}})\cdot\mathbf{E}(t)]\psi(\mathbf{r},t)\ , \tag{1}$$

where $\hat{H}_0$ is the field-free molecular Hamiltonian (i.e., kinetic plus potential-energy operators) and $\boldsymbol{\mu}(\hat{\mathbf{r}})$ is the dipole moment operator. In the laboratory one measures a physical observable $y(t)$, which is the expectation value at time t of the Hermitian operator $\hat{O}$ corresponding to that particular observable:

$$y(t)=\langle\hat{O}\rangle_t=\langle\psi(t)|\hat{O}|\psi(t)\rangle\ , \tag{2}$$

where the operator $\hat{O}$ could also contain an explicit time dependence.

The inverse control problem is expressed as follows. The molecular system is viewed as an input-output system: the input is the external field $\mathbf{E}(t)$, and the output is the expectation value $y(t)$. As such, the molecular system *deterministically* maps an input function into a scalar output function; Eqs. (1) and (2) define the input-output system. The internal state of the input-output system at time t is the wave packet $\psi(\mathbf{r},t)$ and thus the internal state is infinite dimensional. Given an arbitrary external field on the interval $[0,T]$ and the initial condition $\psi(\mathbf{r},0)$, the output $y(t)$ can be computed from Eqs. (1) and (2). The inverse control problem is stated as follows: given a desired output $y_d(t)$ on $[0,T]$ that is the desired time-dependent path, or trajectory, of an expectation value $\langle O\rangle_t$, determine the external field $\mathbf{E}(t)$ on the same interval that will produce it.

The inverse control solution is constructed by differentiating the output [Eq. (2)] with respect to time until the first appearance of the control field $\mathbf{E}(t)$. Here the first derivative of the output $y(t)$ is the equation of motion for the expectation value $\langle\hat{O}\rangle$ (Heisenberg's equation of motion):

$$\frac{d\langle\hat{O}\rangle}{dt}=\frac{1}{i\hbar}\langle[\hat{O},\hat{H}_o]\rangle-\frac{1}{i\hbar}\langle[\hat{O},\boldsymbol{\mu}(\hat{\mathbf{r}})]\rangle\cdot\mathbf{E}(t)+\left\langle\frac{\partial\hat{O}}{\partial t}\right\rangle\ , \tag{3}$$

where $[\hat{O},\hat{H}_0]$ and $[\hat{O},\boldsymbol{\mu}(\hat{\mathbf{r}})]$ denote the commutator of $\hat{O}$ with $\hat{H}_0$ and with $\boldsymbol{\mu}(\hat{\mathbf{r}})$, respectively. [As written, $\mathbf{E}(t)$ is a vector with possibly three independent components; in such a general circumstance, equations of motion for three distinct operators $\hat{O}_x$, $\hat{O}_y$, and $\hat{O}_z$ would be needed for an inversion. More commonly, the field is polarized along a chosen axis $\mathbf{E}(t)=\tilde{\boldsymbol{\epsilon}}E(t)$ and the solution for the simple scalar field $E(t)$ is sought. The more general case will not be considered further here.] The inverse control solution is found by inverting this equation and solving for $E(t)$ and replacing $d\langle\hat{O}\rangle/dt$ with the time derivative of the desired trajectory, dy_d/dt. However, if $[\hat{O},\hat{\boldsymbol{\mu}}\cdot\tilde{\boldsymbol{\epsilon}}]$ is identically zero, then Eq. (3) is not an invertible relation. In such a case, the differentiation must be continued to obtain a higher-order equation which is invertible or, in other words, until the control first appears. To simplify notation we define a sequence of operators ($i=0,1,\ldots$)

$$\hat{O}_{i+1}=\frac{1}{i\hbar}[\hat{O}_i,\hat{H}_0]-\frac{1}{i\hbar}[\hat{O}_i,\hat{\boldsymbol{\mu}}\cdot\tilde{\boldsymbol{\epsilon}}]E(t)+\frac{\partial\hat{O}_i}{\partial t}\ , \tag{4}$$

so that by differentiating the equation of motion (3) i times we obtain

$$\frac{d^{i+1}\langle\hat{O}\rangle}{dt^{i+1}}=\frac{1}{i\hbar}\langle[\hat{O}_i,\hat{H}_0]\rangle-\frac{1}{i\hbar}\langle[\hat{O}_i,\hat{\boldsymbol{\mu}}\cdot\tilde{\boldsymbol{\epsilon}}]\rangle E(t)+\left\langle\frac{\partial\hat{O}_i}{\partial t}\right\rangle\ . \tag{5}$$

Equations of higher and higher order (i.e., increasing i) are constructed until for $i=k$, $\langle[\hat{O}_k,\hat{\boldsymbol{\mu}}\cdot\tilde{\boldsymbol{\epsilon}}]\rangle$ is found to be nonzero ($k+1$ is called the relative order of the system). This provides us with the desired invertible relation between the control and the output as well as its derivatives. Solving Eq. (5) for the field we obtain

$$E(t)=\frac{-i\hbar\dfrac{d^{k+1}y_d(T)}{dt^{k+1}}+\langle[\hat{O}_k,\hat{H}_0]\rangle+i\hbar\left\langle\dfrac{\partial\hat{O}_k}{\partial t}\right\rangle}{\langle[\hat{O}_k,\hat{\boldsymbol{\mu}}\cdot\tilde{\boldsymbol{\epsilon}}]\rangle}\ . \tag{6}$$

Note that for $i=k$, Eq. (5) is a $k+1$ order differential equation whose solution requires $k+1$ initial conditions: $\langle\hat{O}\rangle_{t=0},\{d\langle\hat{O}\rangle/dt\}_{t=0},\ldots,\{d^k\langle\hat{O}\rangle/dt^k\}_{t=0}$. Since the inverse control only serves to ensure that $\{d^{k+1}\langle\hat{O}\rangle/dt\}$ is equal to $\{d^{k+1}y_d/dt^{k+1}\}$ for all t, the initial wave function $\psi(\mathbf{r},0)$ has to be consistent with the $k+1$ initial conditions at $t=0$ for exact tracking.

Knowledge of the wave function $\psi(\mathbf{r},t)$ is required to compute the inverse control field given by Eq. (6). Since direct measurement of the wave function is not possible, $\psi(\mathbf{r},t)$ must be predicted using a mathematical model. For this initial application of the inverse control method to molecular control, we assume that our mathematical model is error free.

The inverted field in Eq. (6) depends upon the wave function $\psi(\mathbf{r},t)$ through the expectation values $\langle[\hat{O}_k,\hat{H}_0]\rangle$ and $\langle[\hat{O}_k,\hat{\boldsymbol{\mu}}\cdot\tilde{\boldsymbol{\epsilon}}]\rangle$, which represent a kind of "feedback" from the system. Thus the field depends explicitly on time through $y_d(t)$ [and $\hat{O}_k(t)$ if the operator $\hat{O}_k$ also has an explicit time dependence] as well as implicitly on time through a functional dependence on $\psi(\mathbf{r},t)$. Taking this into account, Schrödinger's equation (1) can be rewritten as

$$i\hbar\frac{\partial\psi(\mathbf{r},t)}{\partial t}=[\hat{H}_0-\boldsymbol{\mu}(\hat{\mathbf{r}})\cdot\tilde{\boldsymbol{\epsilon}}E(t,\psi(\mathbf{r},t))]\psi(\mathbf{r},t)\ . \tag{7}$$

This is a highly nonlinear differential equation through the extra dependence of $E(t)$ upon $\psi(\mathbf{r},t)$ (i.e., although Schrödinger's equation is normally thought of as linear, in the context of inverse quantum-mechanical control it

is nonlinear). Solution of this equation will yield $\psi(\mathbf{r},t)$, which is substituted back into Eq. (6) to obtain the control field.

The entire inverse control procedure can be understood more clearly if we assume that the time interval $[0,T]$ over which we wish to track our observable is discretized into $N+1$ closely spaced points $t_0,t_1,t_2,\ldots,t_N$, where $t_0=0$ and $t_N=T$. At time t_0 the expectation values in Eq. (6) are computed using the initial wave function $\psi(\mathbf{r},t_0)$. These values along with $\{d^{k+1}y_d/dt^{k+1}\}_{t_0}$ are substituted into Eq. (6) to determine the control field $E(t_0)$. The wave function is then propagated from t_0 to t_1 with Schrödinger's equation (1) using $E(t_0)$. Next the expectation values in Eq. (6) are computed using the wave function $\psi(\mathbf{r},t_1)$, which along with $\{d^{k+1}y_d/dt^{k+1}\}_{t_1}$ are substituted into Eq. (6) to determine $E(t_1)$. The wave function is again propagated from t_1 to t_2 with Schrödinger's equation (1) using $E(t_1)$. This process is repeated until the terminal time t_N is reached and is the basic algorithm used in this work for implementing the inverse control method.

As discussed in Sec. I, much of the recent research pertaining to the quantum-mechanical control has employed optimal control theory [2–4]. It is therefore instructive to compare the inverse control approach of this work to the optimal control approach as applied to the problem of optimal tracking. In the context of the present paper, the natural optimal control functional $\mathcal{J}$ for achieving an objective trajectory $y_d(t)$ in competition with a fluence term weighted by a factor α is

$$\mathcal{J}=\int_0^T[y(t)-y_d(t)]^2dt+\alpha\int_0^T E^2(t)dt \ . \tag{8}$$

This functional is minimized with respect to the control field $E(t)$ subject to the Schrödinger equation (1) and ideally provides an optimal field striking a balance between the tracking goal and the desire to keep the field fluence down. It can be shown that for $\alpha=0$ the optimal control field is the one that results in exact tracking. Inverse control allows for $y(t)$ to be exactly $y_d(t)$; no iteration is called for, but the field $E(t)$ may have undesirable characteristics because there is no simple provision for field restrictions as in the optimal control case (e.g., the fluence penalty).

Past experience has shown that intuition is generally inadequate for determining the field required to achieve a specified value of a molecular observable at a given final time T. The inverse control approach shifts the designer's burden from determining the field to determining the trajectory of the observable leading to the specified value at time T. The designer's intuition may prove more successful in choosing the observable trajectory. Again, for the inverse control approach, the measure of success is the reasonableness of the required field, since $y_d(T)$ will be achieved by design. In using the inverse control approach, one must also be concerned with the so-called zero dynamics [6]. Exact tracking of a desired output trajectory does not ensure that all is well with other aspects of the evolving molecular system. The field required to achieve exact tracking may produce unacceptable behavior in other observables of interest.

Finally, we mention that although often one wants only to achieve a specified value of an observable at a target time T (and therefore one must use the optimal control method to design the control field), in some cases it might be useful to specify an entire objective track instead. For example, if the output $y(t)$ is wildly oscillatory, then problems will arise if the timing of the field with respect to the target time T is slightly skewed because then the output will be far away from the desired value. By prescribing a smooth (as opposed to a wildly oscillatory) track and using the inverse control method to design the field, we can ensure that the transition from the initial system state to the desired final state $y_d(T)$ will be smooth. This may prevent large deviations between the desired value of the observable at time T and the realized value even if the timing is slightly off.

III. APPLICATIONS

In general, the chosen observables to be tracked will depend not only the physical goals we wish to achieve but also on the particular molecule and laboratory constraints. Below we consider some typical cases.

Case (i): $\hat{O}=|m\rangle\langle m|$, a projection operator defined in terms of the mth eigenstate $|m\rangle$ of the zeroth-order Hamiltonian. The prescribed objective trajectory $y_d(t)$ in this case is

$$y_d(t)=y_p(t)=\langle\psi(t)|m\rangle\langle m|\psi(t)\rangle=|c_m(t)|^2 \ , \tag{9}$$

where

$$\psi(\mathbf{r},t)=\sum_n c_n(t)\exp(-i\varepsilon_n t/\hbar)|n\rangle \tag{10}$$

and

$$\hat{H}_0|n\rangle=\varepsilon_n|n\rangle \ . \tag{11}$$

Physically, $y_p(t)$ signifies the tracking of the probability of being in the mth state of the system. A typical chosen trajectory $y_p(t)$ might be a function following a gradual path from $y_p(0)$ to $y_p(T)$ with oscillations corresponding to the natural frequencies of the system. The inverse solution for the field is given by [see Eq. (6)]

$$E(t)=\frac{-i\hbar\dot{y}_p+\langle[|m\rangle\langle m|,\hat{H}_0]\rangle}{\langle[|m\rangle\langle m|,\hat{\boldsymbol{\mu}}\cdot\tilde{\mathbf{e}}]\rangle} \ , \tag{12}$$

with an initial wave function $\psi(\mathbf{r},0)$ chosen such that $\langle\hat{O}\rangle_{t=0}=y_p(0)$.

Case (ii): $\hat{O}=\hat{H}_0$, the energy operator; the objective trajectory here is

$$y_d(t)=y_\varepsilon(t)=\langle\hat{H}_0\rangle_t=\frac{1}{2m}\langle\hat{p}^2\rangle_t+\langle\hat{V}\rangle_t \ , \tag{13}$$

and the inverse solution for the field is given by

$$E(t)=\frac{-2mi\hbar\dot{y}_\varepsilon}{\langle[\hat{p}^2,\hat{\boldsymbol{\mu}}\cdot\tilde{\mathbf{e}}]\rangle} \ , \tag{14}$$

with any initial wave function $\psi(\mathbf{r},0)$ chosen such that $\langle\hat{O}\rangle_{t=0}=y_\varepsilon(0)$.

Case (iii): $\hat{O}=\hat{x}$, the position operator corresponding to the internuclear distance of a particular bond; the ob-

jective trajectory here is

$$y_d(t)=y_x(t)=\langle \hat{x} \rangle_t \ . \tag{15}$$

In this case $[\hat{x},\hat{\mu}]=0$ and hence Eq. (6) cannot be directly employed. As explained in Sec. II, we construct a higher-order operator from Eq. (5), i.e., $\hat{O}_1=[\hat{x},\hat{H}_0]/i\hbar=\hat{p}/m$. The inverse solution for the field is then given by

$$E(t)=\frac{-i\hbar m\ddot{y}_x+\langle [\hat{p},H_0] \rangle}{\langle \hat{p},\hat{\mu}\cdot\vec{\epsilon}] \rangle} \ , \tag{16}$$

with any initial wave function $\psi(\mathbf{r},0)$ chosen such that $\langle \hat{O} \rangle_{t=0}=y_x(0)$ and $\langle d\hat{O}/dt \rangle_{t=0}=\dot{y}_x(0)$.

In both cases (i)and (ii) the field may have multiple isolated singularities due to the denominator passing through zero in Eqs. (12) and (14). For case (iii), the denominator in Eq. (16) is equivalent to the dipole gradient. Here, isolated singularities will arise only if the evolving wave packet significantly samples a region where the dipole moment function reaches an extrema.

It is worth exploring the issue of singularities in more detail since they are likely to occur in many quantum-mechanical inverse control problems. Referring to Eq. (5), it is seen that the dynamical equation remains well behaved even if there is a singularity in the field as long as the product of the field $E(t)$ and the quantity $\langle [\hat{O}_k,\hat{\mu}\cdot\vec{\epsilon}] \rangle$ remains finite. However, numerically a practical problem arises because we must integrate the Schrödinger equation through the singularity in time. The singular behavior of the field results in a very large field amplitude and therefore causes $\psi(\mathbf{r},t)$ to oscillate very rapidly in the region of the singularity and can result in numerical errors. However, in actual calculations where field singularities occur, one virtually never exactly hits the singularity and no real difficulties were encountered due to the finite-time step size of the numerical integration procedure. Most importantly, for the results presented in this work, accurate tracking of $\langle \hat{O} \rangle_t$ was maintained while passing through the singularities. This result clearly implies that the field amplitude near the singularities may be "cut off" to some reasonable finite level and still retain good quality control, as will be demonstrated in Sec. IV. Thus, from a design point of view, the practical significance of attempting to create a near-singular field in the laboratory may not be serious. The important question is how far one may truncate the field amplitude near the singularities and still obtain acceptable tracking results. One could numerically experiment by truncating the field at the singularity to assess the level of field truncation that still leaves a minimal deviation from the objective trajectory. Furthermore, in most real problems the objective trajectory $y_d(t)$ should be viewed as a flexible guide to the desired output; some level of deviation will be acceptable. Some numerical examples of field singularities will be shown in the following section.

Finally, in relation to the above discussion it is instructive to return to the optimal control formulation in Eq. (8). The presence of the fluence term with $\alpha\neq 0$ assures that the field solution is "well behaved," but at the perhaps minor expense of $\langle \hat{O} \rangle_t$ not exactly tracking $y_d(t)$ (and the additional hidden expense of iteratively finding the field). One sees then that the singularities may arise from the demand of *exact* tracking of $y_d(t)$ with inverse control. However, in the vicinity of $y_d(t)$ there will likely be other trajectories that exhibit no singularities. It is then a practical matter to explore the balance between the desired output trajectory and desirable field behavior.

IV. ILLUSTRATIONS

Here we apply the inverse control formalism to position and energy tracking on the hydrogen fluoride molecule which here is modeled as a nonrotating Morse oscillator [11]. Specifically, the interaction potential is

$$V(x)=D\{1.0-\exp[-\beta(x-x_{\rm eq})]\}^2 \ , \tag{17}$$

and the dipole moment is

$$\mu(x)=Bx\exp(-\zeta x^4) \ . \tag{18}$$

The parameters of the Morse potential $V(x)$ and the dipole moment $\mu(x)$ are the same as those in Ref. [11]. Integration of Schrödinger's equation is performed using the split-operator scheme [12] and exponentiation of the kinetic-energy operator is performed using the fast Fourier transform (FFT) algorithm [13]. Convergence with respect to grid point spacing and time step was checked. Atomic units are used throughout this section.

A. Position tracking

Here $\hat{O}=\hat{x}$ [case (iii) in Sec. III] and for this one-dimensional problem the expression for the control field for position tracking is [cf. Eq. (16)]

$$E(t)=\frac{m\ddot{y}_x+\left\langle \frac{dV(\hat{x})}{dx} \right\rangle}{\left\langle \frac{d\mu(\hat{x})}{dx} \right\rangle} \ . \tag{19}$$

The objective trajectory is the internuclear distance $y_d t)=y_x(t)$. This tracking trajectory could be imposed with any logic, including digitization of a smoothly drawn curve. Here the following classical equation of motion for an antidamped oscillator is used to generate the trajectory:

$$m\ddot{y}_x=-\frac{dV(y_x)}{dy_x}+\gamma\dot{y}_x \ , \tag{20}$$

where m is the reduced mass of the oscillator and $\gamma>0$. The solution of the above equation is used only as an artificial device to generate a suitable smooth trajectory for $y_x(t)$. Similar devices have also been employed to generate goal dynamics in studies of classically nonlinear driven oscillators [14]. The advantage of using Eq. (20) is that since the interaction potential $V(y_x)$ is the same as that of the actual system, the trajectory $y_x(t)$ thus generated has oscillations at the natural frequency of the system.

As previously discussed in Sec. III, the initial condi-

tions of the generated trajectory $y_x(0)$ and $\dot{y}_x(0)$ must match the corresponding expectation values of the initial wave packet, $\langle \hat{x} \rangle_{t=0}$ and $\langle \hat{p} \rangle_{t=0}$. Here, the initial wave packet was simply the ground vibrational eigenstate of the hydrogen fluoride (HF) potential, which is a reasonable assumption if the system is at room temperature. The position and momentum expectation values of this wave packet, 1.77 and 0.0, respectively, were used as the initial conditions for solving Eq. (20). (Changing the initial wave packet to, for instance a Gaussian centered at the same initial position, does not qualitatively change the results, though the inverse field obtained is different.)

Before presenting numerical results, a few conclusions can be drawn about the nature of the control field from Eq. (19) if the objective trajectory $y_x(t)$ is generated from Eq. (20). Substituting Eq. (20) into Eq. (19), the control field becomes

$$E(t)=\frac{\gamma\dot{y}_x-\dfrac{dV(y_x)}{dy_x}+\left\langle\dfrac{dV(\hat{x})}{dx}\right\rangle}{\left\langle\dfrac{d\mu(\hat{x})}{dx}\right\rangle} . \tag{21}$$

If the potential is harmonic, then $\langle dV(\hat{x})/dx \rangle = dV(y_x)/dy_x$ at all times. Assuming the dipole gradient can be approximated by a constant α [i.e., $\mu(x)\approx\alpha x$], the control field is

$$E(t)=\gamma\dot{y}_x\alpha . \tag{22}$$

Since the solution for Eq. (20) with a harmonic potential is of the form

$$y_x(t)=A\exp(\gamma t)\sin(\omega_{\text{harm}}t+\theta) , \tag{23}$$

where ω_{harm} is the natural frequency of the harmonic oscillator, then by Eq. (22) the control field is also an oscillating function of frequency ω_{harm} multiplied by an exponentially rising amplitude. This conclusion was borne out numerically (not shown here).

Now consider the case of an anharmonic potential which is "hard" for $x<x_{\text{eq}}$ and "soft" for $x>x_{\text{eq}}$ (i.e., like a Morse potential):

$$V(x)=\tfrac{1}{2}k(x-x_{\text{eq}})^2-\tfrac{1}{6}k'(x-x_{\text{eq}})^3+\tfrac{1}{24}k''(x-x_{\text{eq}})^4-\cdots , \tag{24}$$

where $k,k',k'',\ldots>0$. Considering only the first two terms in Eq. (24), the classical potential gradient is

$$\frac{dV(y_x)}{dy_x}=k(y_x-x_{\text{eq}})-\tfrac{1}{2}k'(y_x-x_{\text{eq}})^2 , \tag{25}$$

and the corresponding quantum expectation value is

$$\left\langle\frac{dV(\hat{x})}{dx}\right\rangle=k(\langle\hat{x}\rangle-x_{\text{eq}})-\tfrac{1}{2}k'\langle(\hat{x}-x_{\text{eq}})^2\rangle . \tag{26}$$

Assuming that the norm of the wave function is one and the growth term γ is relatively small, i.e., $\gamma|\dot{y}_x|\ll|dV(y_x)/dy_x|$, $|\langle dV(\hat{x})/dx\rangle|$, and also noting that $y_x(t)=\langle\hat{x}\rangle$, for all t *by construction* of the inverse control problem for position tracking, then Eq. (21) becomes

$$E(t)=\frac{-k'\langle(\hat{x}-\langle\hat{x}\rangle)^2\rangle}{2\alpha} . \tag{27}$$

Thus the control field possesses a strong (negative) dc component and never changes sign, since it is proportional to the negative variance of the wave function. Also, we can predict within this approximation that as the wave packet acquires more energy and becomes more delocalized, this dc field component will also increase.

We now turn to numerical results where, as in all of the numerical calculations in this work, we employ the HF Morse potential [Eq. (17)] and dipole moment [Eq. (18)] in the integration of Schrödinger's equation. Figure 1 shows the objective trajectory $y_x(t)$ generated from Eq. (20) using $\gamma=1.0$. The potential $V(y_x)$ used for integrating Eq. (20) is identical to the HF Morse potential. Superimposed on $y_x(t)$ in Fig. 1 is the achieved trajectory $\langle x\rangle_t$, obtained from propagating Schrödinger's equation using the inverse control field [computed from Eq. (19)] shown in Fig. 2. Note that the tracking is perfect, i.e., $y_x(t)$ and $\langle\hat{x}\rangle_t$ are identical. Note also the presence of a strong (negative) dc component in the field which increases throughout the pulse length. This rise in field strength corresponds with a similar increase in energy, as seen in Fig. 3, which plots the energy expectation value $\langle\hat{H}_0\rangle_t$. This correspondence can be rationalized by examining the equation of motion for $\langle\hat{H}_0\rangle$ [assuming $\mu(x)\approx\alpha x$]:

$$\frac{d\langle\hat{H}_0\rangle}{dt}=\frac{E(t)\langle\hat{p}\rangle\alpha}{m} . \tag{28}$$

Thus as the field amplitude increases, so does $d\langle\hat{H}_0\rangle/dt$ and therefore $\langle\hat{H}_0\rangle$; this in turn further delocalizes the wave packet and increases the variance. By Eq. (27) this increases the field amplitude further. Thus if the momentum of the wave packet is large enough, this process will

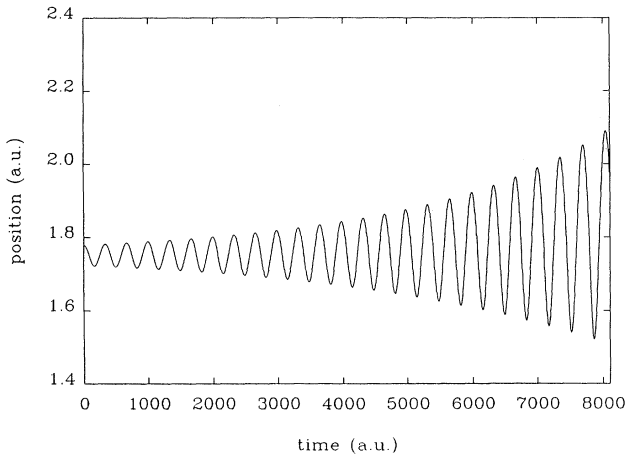

FIG. 1. The objective position trajectory $y_x(t)$ generated from the equation of motion for a classical driven oscillator [Eq. (20)] with $\gamma=1.0$. The potential $V(y_x)$ used to generate $y_x(t)$ was the same as the HF Morse potential (see text). Superimposed on this is the achieved trajectory $\langle\hat{x}\rangle_t$. Note that the two trajectories are virtually identical.

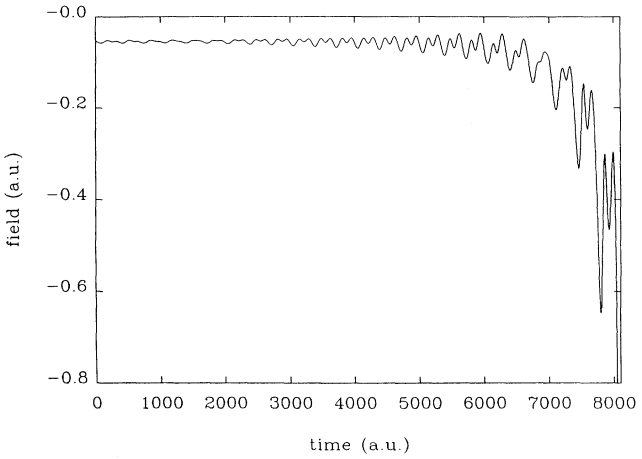

FIG. 2. The inverse solution for the control field for the position trajectory shown in Fig. 1. The field reaches a maximum amplitude of -2.9 a.u. at the end of the pulse.

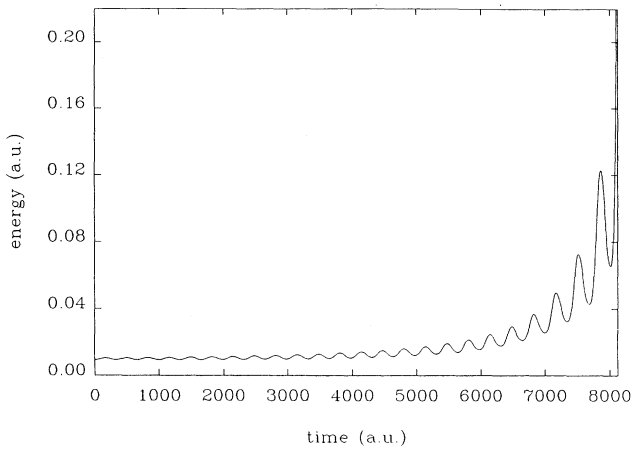

FIG. 3. The energy expectation value $\langle \hat{H}_0 \rangle$ as a function of time corresponding to the position trajectory shown in Fig. 1.

result in the exponential-like growth of the field intensity and the energy expectation value, as shown in Figs. 2 and 3.

More physical insight into the origin of the strong dc component can be gained as follows. The initial wave packet $\psi(\mathbf{r},0)$ is a stationary state (since it is composed of only the ground vibrational eigenstate) and thus the expectation value of its position and momentum (or any other operator) does not change with time. Therefore, by Ehrenfest's theorem,

$$\frac{d\langle \hat{p} \rangle}{dt} = -m\left\langle \frac{dV(\hat{x})}{dx} \right\rangle , \tag{29}$$

we know that $\langle dV(\hat{x})/dx \rangle_{t=0}$ is zero. However, because the potential is anharmonic, $\langle \hat{x} \rangle_{t=0} \neq x_{\mathrm{eq}}$. The initial condition of the objective trajectory $y_x(0)$ used in Eq. (20) must be equivalent to $\langle \hat{x} \rangle_{t=0}$ and thus the potential gradient felt by the classical particle at $t=0$, i.e., $\{dV(y_x)/dy_x\}_{t=0}$, is not zero. The control field compensates for this discrepancy by using a (negative) dc field component E_{dc} to add an "artificial" potential $-\mu(\hat{x})\cdot E_{\mathrm{dc}}$ to the Hamiltonian in Eq. (1). Indeed, at $t=0$ it is found that

$$-\left\langle \frac{d\mu(\hat{x})}{dx} \right\rangle E_{\mathrm{dc}} \approx \frac{dV(y_x)}{dy_x} , \tag{30}$$

showing that the dc component creates an "artificial" potential gradient for the initial wave packet. At later times the negative dc component persists because, at least for small-amplitude oscillations, the classical potential gradient remains significantly smaller than its corresponding expectation value, as seen in Fig. 4, where we plot $\{dV(y_x)/dy_x\}_t$ (dotted line) and $\langle dV(\hat{x})/dx \rangle_t$ (solid line). This can be explained by the fact that the wave packed $\psi(\mathbf{r},t)$ possesses a spatial width and thus samples a region of the potential gradient unlike the classical particle for which the gradient is computed at one specific point. If the wave packet is assumed to be roughly a Gaussian at low energies with its center matching the classical position $y_x(t)$, then $\langle dV(\hat{x})/dx \rangle_t$ will be less than $\{dV(y_x)/dy_x\}_t$ due to the asymmetry of the potential well. At higher energies, however, the wave packet becomes more delocalized and its shape more irregular, thereby complicating the analysis.

One possible way of avoiding the undesirable dc component is to use a "shifted" potential for generating the tracking (classical) trajectory, for example, a potential of the form

$$V(y_x) = \tfrac{1}{2}k(y_x - \bar{x}_{\mathrm{eq}})^2 - \tfrac{1}{6}k'(y_x - \bar{x}_{\mathrm{eq}})^3 , \tag{31}$$

where $\bar{x}_{\mathrm{eq}} > x_{\mathrm{eq}}$. Equation (21) then becomes [assuming the growth term γ is relatively small as in Eq. (27)]

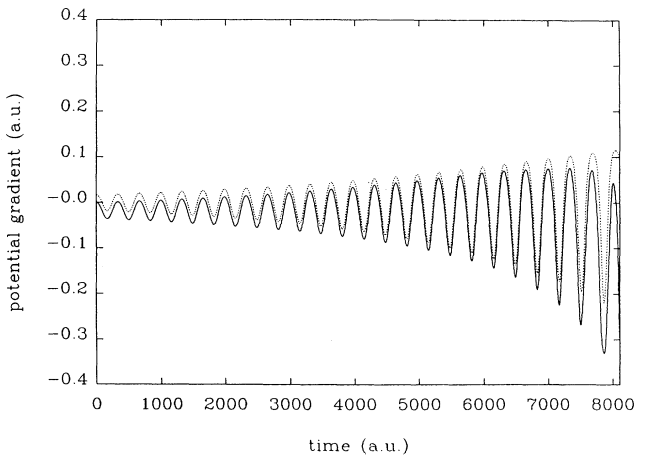

FIG. 4. Classical potential gradient $\{dV(y_x)/dy_x\}$ (dotted line) and the corresponding quantum expectation value $\langle dV(\hat{x})/dx \rangle$ (solid line) as a function of time for the position trajectory shown in Fig. 1.

$$E(t)=\frac{k(\bar{x}_{\rm eq}-x_{\rm eq})+\frac{1}{2}k'(\bar{x}_{\rm eq}^2-x_{\rm eq}^2)-k'\langle(\hat{x}-\langle\hat{x}\rangle)^2\rangle}{2\alpha} . \tag{32}$$

Since $\bar{x}_{\rm eq}-x_{\rm eq}>0$, the first two terms of the numerator of Eq. (32) will help to cancel the negative variance in the control field. In more physical terms, note that if $\bar{x}_{\rm eq}=\langle\hat{x}\rangle_{t=0}$, then the potential gradient felt by the classical particle at $t=0$, i.e., $\{dV(y_x)/dy_x\}_{t=0}$, will be zero; this avoids the need to create an artificial potential gradient with the dc field component as before.

Taking into account these remarks, we carry out another position tracking control exactly as before (except here $\gamma=4.0$) but this time using a shifted Morse potential for the classical integration, i.e.,

$$V(y_x)=D\{1.0-\exp[-\beta(y_x-\bar{x}_{\rm eq})]\}^2 , \tag{33}$$

where $\bar{x}_{\rm eq}=\langle\hat{x}\rangle_{t=0}+10^{-8}$. [Remembering that the initial momentum $\dot{y}_x(0)=0.0$, we cannot set $x_{\rm eq}$ to be *exactly* $\langle\hat{x}\rangle_{t=0}$ because then $\{dV(y_x)/dy_x\}_{t=0}$ would be *exactly* zero and thus prevent the classical particle from moving at all from its initial position $y_x(0)$.] In Fig. 5 we plot the objective trajectory $y_x(t)$ and the achieved trajectory $\langle\hat{x}\rangle_t$ using the inverse control field shown in Fig. 6. (The initial 11 000 units of time in these plots are not shown because of the very-low-amplitude motion during this time.) As in the unshifted potential case, the objective trajectory $y_x(t)$ and the realized trajectory $\langle\hat{x}\rangle_t$ are virtually identical. Note that the field in this case, however, is not negatively biased until near the end of the pulse. It is apparent then, as predicted in Eq. (32), that the shifted potential [Eq. (33)] used in the classical integration helps to suppress the dc component temporarily. However, as the expectation value of the energy becomes larger and larger [see Figs. 7(a) and 7(b)], the increasing variance of the wave packet will begin to more

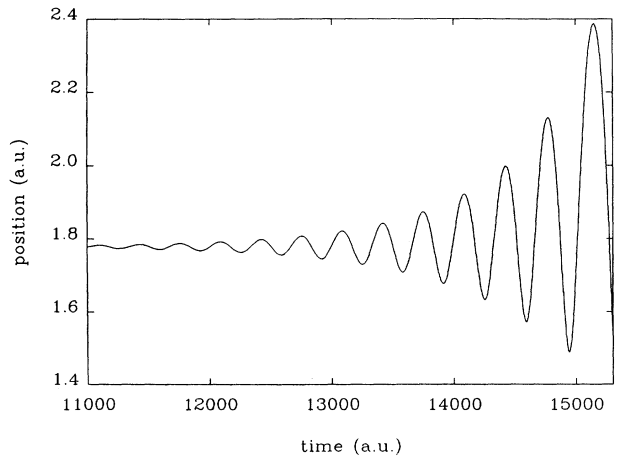

FIG. 5. Same as Fig. 1 except here a "shifted" Morse potential (see text) was used in generating the objective trajectory $y_x(t)$. As in the case shown in Fig. 1, the objective and achieved trajectories are virtually identical.

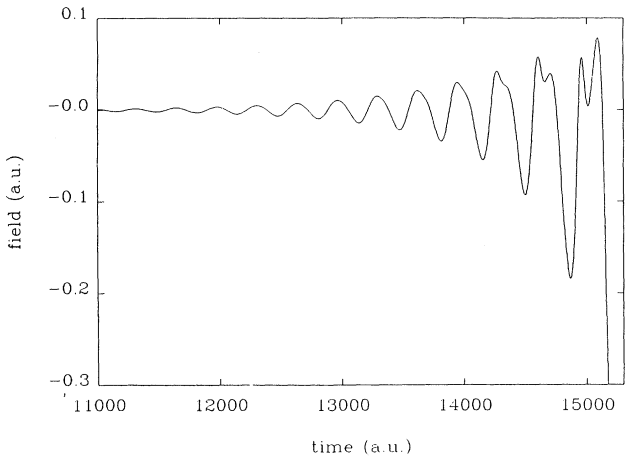

FIG. 6. The inverse solution for the control field for the position trajectory shown in Fig. 5. The field reaches a maximum amplitude of -1.2 a.u. at the end of the pulse.

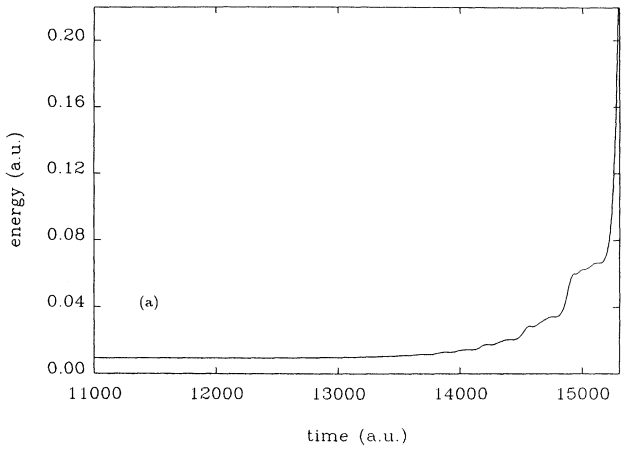

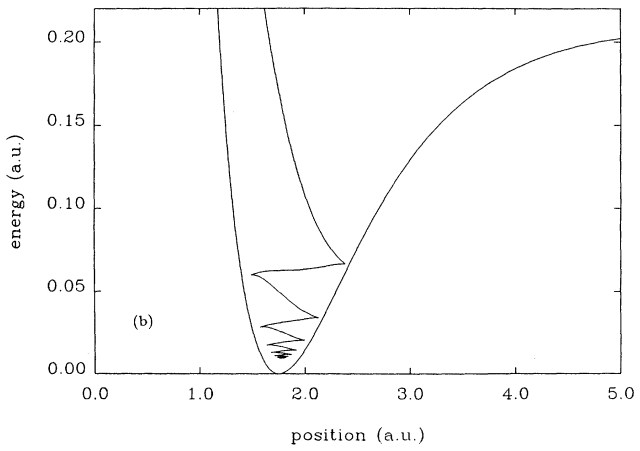

FIG. 7. The energy expectation value $\langle\hat{H}_0\rangle$ as a function of (a) time and (b) position in the HF potential well corresponding to the position trajectory shown in Fig. 5.

than offset the shifted potential modification.

A more detailed examination of the control field and its interaction with the HF system provides physical insight as to how the objective trajectory in Fig. 5 is realized. Besides the previously mentioned dc component, a power spectrum of the field (Fig. 8) reveals a dominant frequency component at ≈ 0.018 as well as smaller ones at ≈ 0.036 and ≈ 0.053. These values correspond, respectively, to the fundamental $(0 \rightarrow 1)$ vibrational transition and the first $(0 \rightarrow 2)$ and second $(0 \rightarrow 3)$ overtone transitions of HF. Clearly, the control field utilizes transitions among the first few vibrational eigenstates in order to produce the objective trajectory in Fig. 5. This is also reflected in the populations of the lower eigenstates plotted against time in Fig. 9. Since the initial wave packet $\psi(\mathbf{r},0)$ is the first vibrational eigenstate, the population of this state remains significantly high until much later times and explains why the first fundamental contributes a dominant component to the field. However, as other states become significantly populated, the overtones become more important.

In our second example of position tracking we consider a case where the expectation value of the dipole gradient crosses zero and thereby produces a singularity in the inverse control field [see Eq. (19)]. The objective trajectory $y_x(t)$ is again generated using Eq. (20) with the same initial conditions and employing the shifted Morse potential [Eq. (33)]. However, here we set $\gamma = 12.0$ to produce higher-amplitude oscillations in the trajectory. Figure 10 shows the objective trajectory $y_x(t)$ (dotted line) and the achieved trajectory $\langle \hat{x} \rangle_t$ (solid line). (The initial 4500 units of time in these plots are not shown because of the very-low-amplitude motion during this time.) A limit (2.0) was imposed on the magnitude of the amplitude of the inverse control field (Fig. 11). From comparing the field with a plot of the dipole gradient expectation value versus time (Fig. 12) one notes that the field singularity at $t \approx 5180$ corresponds to the time when $\langle d\mu(\hat{x})/dx \rangle$ is zero, as expected. The maximum deviation of the achieved trajectory $\langle \hat{x} \rangle_t$ from the objective trajectory $y_x(t)$ is 2.1 percent, which occurs at the end of the pulse.

As expected, less-stringent field restrictions result in better tracking. For example, an inversion performed with a field cutoff of 5.0 (not shown here) produced a tracking deviation of 1.0 percent. Another inversion performed with no explicit limit imposed on the amplitude of the control field resulted in a tracking deviation of only 0.04 percent (an effective limit occurred due to the finite time step used in the numerical integration procedure). In this case, however, the field amplitude reaches an unreasonably large maximum of 17.0 at the time closest to that where the singularity occurs. These results show that for this case the field amplitude may be "cut off" to an acceptable value at the singularity and still achieve reasonable results.

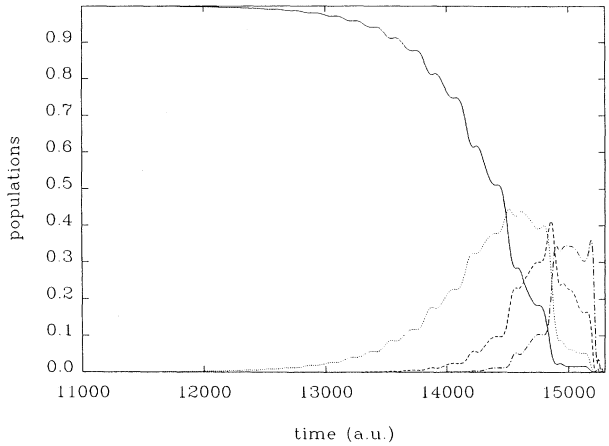

FIG. 9. First (solid line), second (dotted line), third (dashed line), and fourth (dotted-dashed line) vibrational eigenstate populations of HF as a function of time while the bond follows the trajectory shown in Fig. 5.

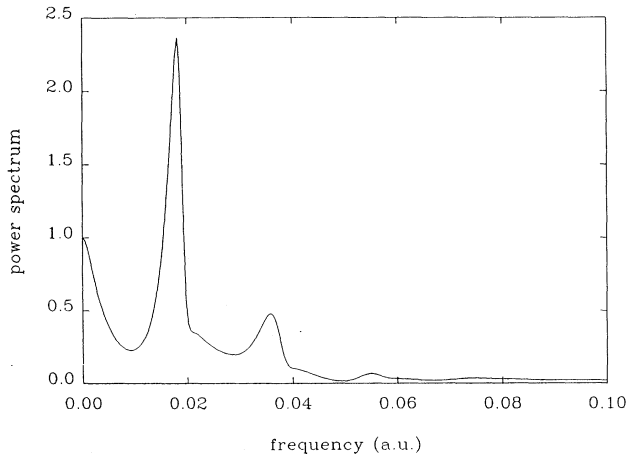

FIG. 8. The power spectrum of the control field shown in Fig. 6. The dominant peak at $\omega \approx 0.018$ a.u. corresponds to the first fundamental $(0 \rightarrow 1)$ vibrational transition of the HF molecule. The smaller peaks of higher frequency correspond to various overtone transitions from the ground state.

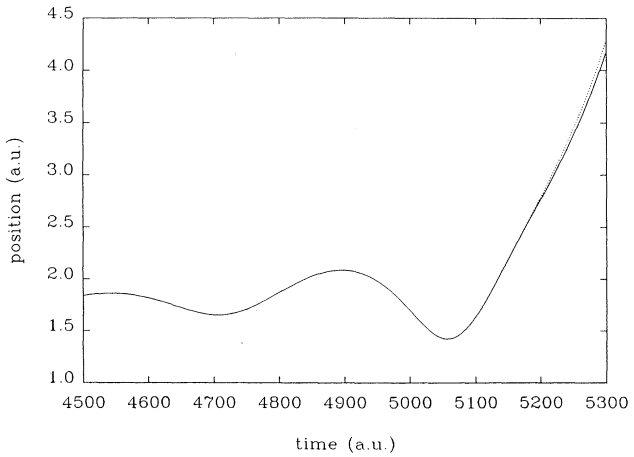

FIG. 10. The objective position trajectory $y_x(t)$ (dotted line) and the achieved trajectory $\langle \hat{x} \rangle_t$ (solid line) where, as for the case shown in Fig. 5, a "shifted" Morse potential was used to generate $y_x(t)$. Here, however, $\gamma = 12.0$ a.u.

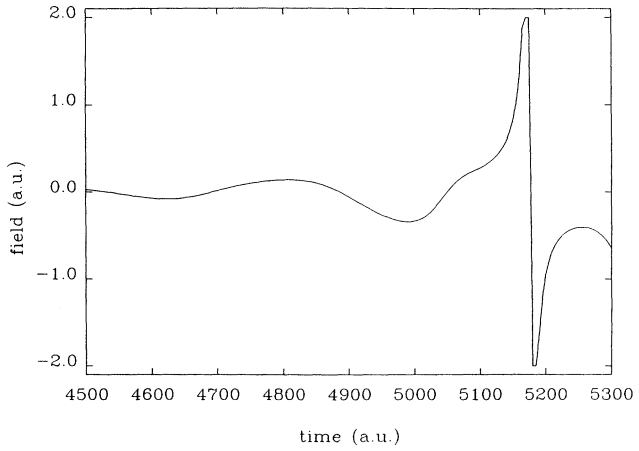

FIG. 11. The inverse solution for the control field for the position trajectory shown in Fig. 10. A limit of 2.0 a.u. was imposed on the magnitude of the control field amplitude (see text). Despite the appearance of the singularity at $t \approx 5180$ a.u., reasonably precise tracking is still maintained.

B. Energy tracking

Here $\hat{O}=\hat{H}_0$ [case (ii) in Sec. III] and the expression for the control field for the one-dimensional problem is [cf. Eq. (14)]

$$E(t)=\frac{2m\dot{y}_\varepsilon}{2\left\langle \frac{d\mu(\hat{x})}{dx}\hat{p}\right\rangle - i\hbar\left\langle \frac{d^2\mu(\hat{x})}{dx^2}\right\rangle} . \tag{34}$$

The objective trajectory $y_d(t)=y_\varepsilon(t)$ was obtained by again integrating the equation of motion for an anti-damped oscillator [Eq. (20)] and simultaneously computing its energy:

$$y_\varepsilon(t)=\tfrac{1}{2}m[\dot{y}_x(t)]^2+V(y_x(t)) . \tag{35}$$

Before turning to numerical results we can draw some conclusions about the nature of the control field from Eq. (34). Assuming $\mu(x)\approx\alpha x$ and realizing that $\dot{y}_\varepsilon(t)=\gamma[\dot{y}_x(t)]^2$, Eq. (34) becomes

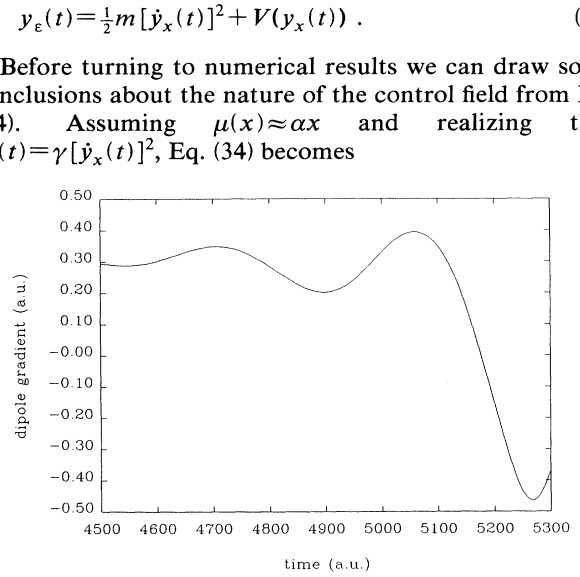

FIG. 12. The expectation value of the gradient of the dipole moment for the system evolving on the trajectory shown in Fig. 10.

$$E(t)=\frac{2m\gamma[\dot{y}_x(t)]^2}{\alpha\langle\hat{p}\rangle} . \tag{36}$$

Making the approximation that $m\dot{y}_x(t)=C\langle\hat{p}\rangle_t$, i.e., the momentum expectation value oscillates with the same frequency as the momentum of the classical oscillator, we then have

$$E(t)=\frac{2C\gamma\dot{y}_x(t)}{\alpha} . \tag{37}$$

The frequency of the oscillator is a function of energy (because the potential is anharmonic) and therefore so is the trajectory $y_x(t)$ and its time derivative $\dot{y}_x(t)$. Since the energy increases with time, we may write $\omega(\varepsilon)=\omega(\varepsilon(t))$, and the inverse control field takes on the form

$$E(t)\approx\sum_n A_n(t)\cos[\omega_n(t)t+\delta_n(t)] , \tag{38}$$

where δ_n is a phase. Thus we see from Eq. (38) that chirping is a natural solution to molecular energy tracking control. This is consistent with the suggestion of using chirped fields to vibrationally excite anharmonic systems, as shown in recent studies by other workers [15]. The chirped field solution can also be realized from the nature of the control field in the position tracking case. Here, $\langle\hat{x}\rangle_t$ oscillates at progressively smaller frequencies as the energy increases, and by Eq. (27) the control field should reflect this behavior.

We now turn to numerical results for inverse control of energy tracking. Here there was no need to employ a shifted potential as in the position tracking cases and so the potential $V(y_x)$ used in Eq. (20) was the same as the HF Morse potential [Eq. (17)] used for integrating Schrödinger's equation. The initial position $y_x(0)$ was slightly altered from 1.77 to 1.94 so that the initial condition of the objective trajectory $y_\varepsilon(0)=V(y_x(0))$ was equal to the energy of the initial wave packet $\langle\hat{H}_0\rangle_{t=0}$. For all energy tracking results the growth term γ was set at 2.5.

Unlike the position tracking inversion, the control field given by Eq. (34) is likely to have multiple singularities. These correspond to multiple roots in the denominator of Eq. (34) which occur whenever (approximately) the wave-packet momentum $\langle\hat{p}\rangle_t$ is zero. To avoid numerical blowups, a small term η was added to the denominator of Eq. (34) with the sign rationalized. This procedure should be distinguished from the position tracking case in the previous section where a specified limit was imposed on the magnitude of the field amplitude. In the energy tracking case here the inverse control field explicitly depends on the η damping parameter as opposed to being truncated to a specified value.

Figure 13(a) shows the objective energy trajectory $y_\varepsilon(t)$ (dotted line) and the achieved trajectory $\langle\hat{H}_0\rangle_t$ (solid line) produced from the inverse control field shown in Fig. 13(b) for $\eta=0.001$. Figures 14(a) and 14(b) show similar plots for $\eta=0.1$. As expected, the deviation of the realized trajectory $\langle\hat{H}_0\rangle_t$ from the objective trajectory $y_\varepsilon(t)$ in the $\eta=0.001$ case is much smaller than for the $\eta=0.1$ case. However, a price is paid for the higher pre-

cision in that the control field in Fig. 13(b) exhibits the effects of the singularities more, resulting in a more fragmented field structure. On the other hand, the field for the $\eta=0.1$ case [Fig. 14(b)] is much smoother and possesses a lower peak field amplitude, although the tracking is not as precise. However, it is likely that in practical situations exact tracking often will not be required. For example, if the actual goal here was to simply excite the HF molecule up to its dissociation energy ($D=0.21$), both fields accomplish this task, but the field in Fig. 14(b) is obviously more desirable from an experimental point of view.

To determine if the resultant control fields for energy tracking exhibit chirping behavior, power spectrums were computed of the first half ($t\in[0,1023]$) of the control field shown in Fig. 13(b) (the solid line in Fig.15) and of the second half ($t\in[1024,2047]$) (the dotted line in Fig. 15). The dominant frequency of the second half of the control field, $\omega\approx 0.012$, which approximately corresponds to the $(7\rightarrow 8)$ vibrational transition, is significantly less than the dominant frequency of the first half, $\omega\approx 0.018$, which corresponds to the $(0\rightarrow 1)$ transi-

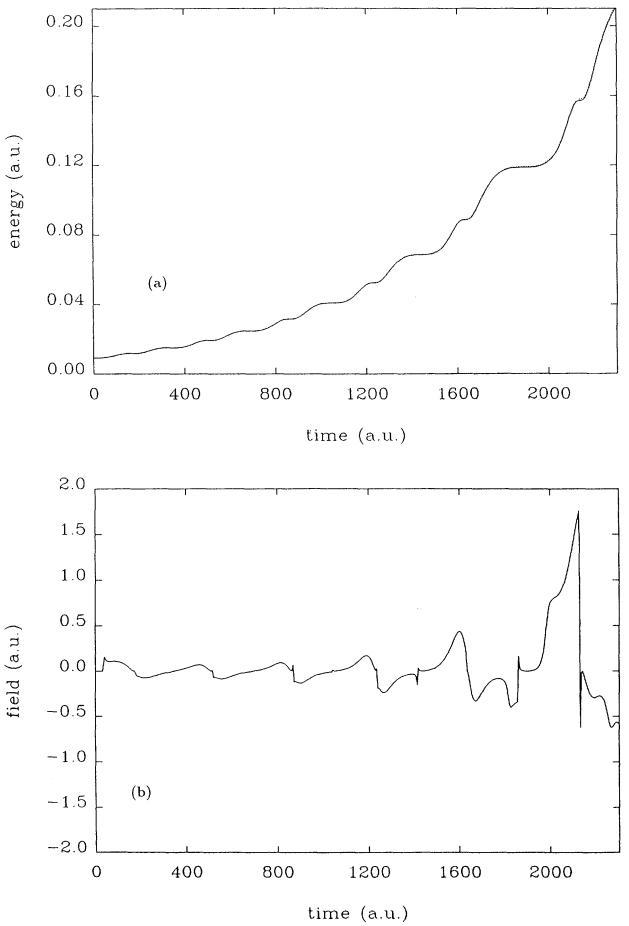

FIG. 13. (a) Objective energy trajectory $y_\varepsilon(t)$ (dotted line) and achieved trajectory $\langle\hat{H}_0\rangle_t$ (solid line) for $\eta=0.001$ (see text). (b) The corresponding inverse solution for the control field [computed from Eq. (34)].

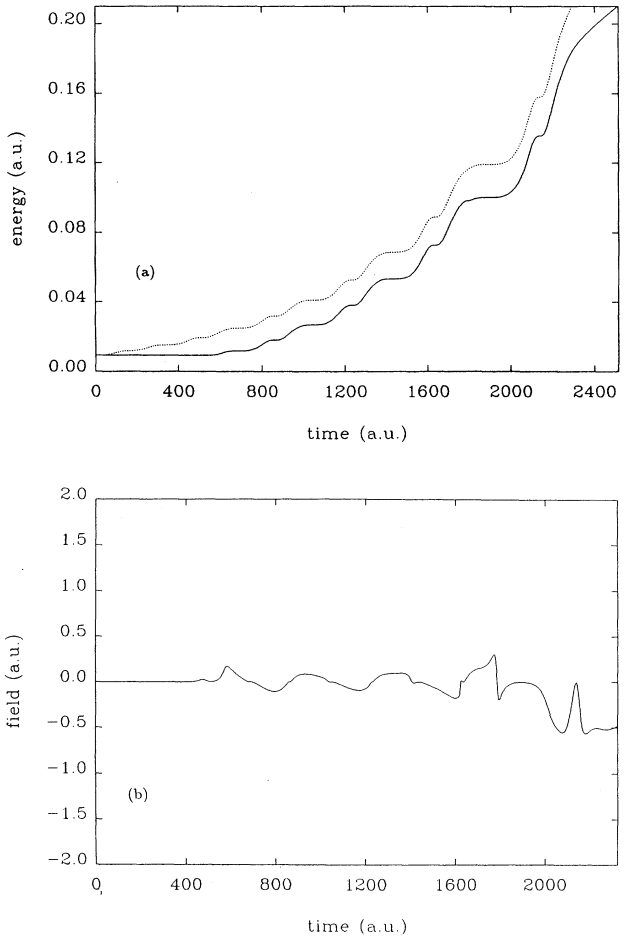

FIG. 14. (a) Same as Fig. 13(a) except $\eta=0.1$ Note that although the tracking here is not as precise as in Fig. 13(a), the control field here [Fig. 14(b)] is more amenable to experimental implementation.

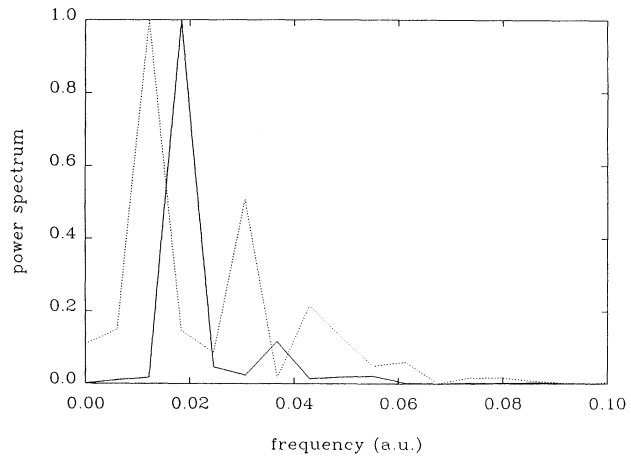

FIG. 15. Power spectrums of the first half (solid line) and the second half (dotted line) of the control field shown in Fig. 13(b).

tion. (The smaller peaks in both plots correspond to various overtone transitions.) This change of dominant frequency components with time is indicative of chirping behavior.

V. CONCLUSIONS

In this paper we have formulated the theory of inverse quantum-mechanical control and applied it to a diatomic system for two different goals. Our results for the problem of position tracking show that the method is remarkably successful in producing an inverse solution for the external field that reproduces a desired trajectory. The results for the energy tracking show that the multiple singularities in the control field may arise and thereby perhaps tax one's intuition in choosing an appropriate input trajectory, but still the tracking in most cases is remarkably precise. The singularities may be truncated to give reasonable tracking, as shown.

In principle, the inverse control method may be useful for designing experiments. A much more thorough study of the method is needed, including further illustrations, to establish its full utility. At a minimum, inverse tracking should be regarded as a useful device in testing and improving one's intuition in designing molecular control fields. A major advantage of inverse control is its lack of iteration to achieve a field design. This makes the method potentially quite attractive for the study of controlling polyatomic systems where the numerical computations are more expensive. In this case the issue of tracking multiple objectives needs to be carefully examined. A suggestion in this regard is given in the Appendix. With the methodology introduced in this paper we hope to have established an alternative direction in the control of reactive quantum-mechanical systems.

ACKNOWLEDGMENTS

We thank Mr. Yu Chen for helpful discussions on this project. We also acknowledge support for this research from the U.S. Air Force Office of Scientific Research and the U.S. Army Research Office.

APPENDIX: INVERSION CONTROL OF POLYATOMIC MOLECULES: THE STROBOSCOPIC METHOD

For a polyatomic molecule, the dynamics of the various local modes cannot be treated independently. Here we write the total Hamiltonian as consisting of the kinetic-energy terms involving momenta corresponding to the local modes as well as cross terms that describe the coupling between modes and an interaction potential which is a function of the position coordinates of all the modes. In general,

$$\hat{H}=\tfrac{1}{2}\hat{\mathbf{p}}^T\mathbf{G}\hat{\mathbf{p}}+V(\hat{\mathbf{q}})-\boldsymbol{\mu}(\hat{\mathbf{q}})\cdot\mathbf{E}(t)\ , \tag{A1}$$

where the interaction with the external field has also been included. The matrix $\mathbf{G}$ is symmetric and its elements involve the masses of the atoms in the molecule. The inverse tracking formulation introduced in Sec. III can, in principle, be applied directly to polyatomic systems. In such a case, $\hat{O}$ would be chosen and the procedure immediately follows. However, a special problem can arise, as may be seen from a simple example when $\hat{O}=\hat{r}_i$ is taken as the ith bond length coordinate. Tracking $\langle\hat{r}_i\rangle=y_d^i(t)$ could be prescribed, but there is no explicit control over the other internal coordinate expectation values $\langle\hat{r}_j\rangle_t$, $j\neq i$. Thus one might specify $y_d^i(t)$ to break the ith bond, but the resultant $\mathbf{E}(t)$ might also unwittingly break other bonds as would only be discovered after performing the inverse control design. In general, we would like to control, as best as possible, N distinct operators $\hat{O}_j$, $j=1,\ldots,N$. Arbitrary *individual* specification of $y_d^j(t)$ will, in general, yield N inconsistent fields $\mathbf{E}_j(t)$, $j=1,\ldots,N$. We suggest below a possible means to circumvent this problem.

A general invertible relation for tracking multiple operators is developed as follows. Consider the linear combination of operators $\hat{O}$:

$$\hat{O}=\sum_{j=1}^{N}w_j(t)\hat{O}_j\ , \tag{A2}$$

which we now treat as the object to be controlled with $w_j(t)$ to be specified. Then the objective is given by

$$y_d(t)=\langle\hat{O}\rangle_t=\sum_{j=1}^{N}w_j(t)y_d^j(t)\ , \tag{A3}$$

where

$$y_d^j(t)=\langle\hat{O}_j\rangle_t\ . \tag{A4}$$

Differentiating Eq. (A2) with respect to time gives

$$i\hbar\frac{d\langle\hat{O}\rangle}{dt}=i\hbar\sum_{j=1}^{N}\dot{w}_j(t)y_d^j(t)+i\hbar\sum_{j=1}^{N}w_j(t)\frac{dy_d^j(t)}{dt}\ . \tag{A5}$$

Substituting Eq. (A2) into Eq. (3) we have

$$\begin{aligned}i\hbar\frac{d\langle\hat{O}\rangle}{dt}=&\sum_{j=1}^{N}w_j(t)\langle[\hat{O}_j,\hat{H}_0]\rangle-\sum_{j=1}^{N}w_j(t)\langle[\hat{O}_j,\hat{\boldsymbol{\mu}}]\rangle\cdot\mathbf{E}(t)\\&+i\hbar\sum_{j=1}^{N}\dot{w}_j(t)y_d^j(t)\\&+i\hbar\sum_{j=1}^{N}w_j(t)\left\langle\frac{\partial\hat{O}_j}{\partial t}\right\rangle\ .\end{aligned} \tag{A6}$$

Finally, subtracting Eq. (A5) from Eq. (A6) we obtain

$$\begin{aligned}i\hbar\sum_{j=1}^{N}w_j(t)\frac{dy_d^j(t)}{dt}=\sum_{j=1}^{N}w_j(t)\Bigg[&\langle[\hat{O}_j,\overline{H}_0]\rangle\\&-\langle[\hat{O}_j,\hat{\boldsymbol{\mu}}]\rangle\cdot\mathbf{E}(t)\\&+i\hbar\left\langle\frac{\partial\hat{O}_j}{\partial t}\right\rangle\Bigg]\ .\end{aligned} \tag{A7}$$

Assuming that during any particular time interval $[t_i,t_i+\tau]$ only one weight, say $w_i(t)$ here, is nonzero, immediately leads to the conclusion

$$i\hbar\frac{dy_d^i(t)}{dt}=\langle[\hat{O}_i,\hat{H}_0]\rangle-\langle[\hat{O}_i,\hat{\boldsymbol{\mu}}]\rangle\cdot\mathbf{E}(t)+i\hbar\left\langle\frac{\partial\hat{O}_i}{\partial t}\right\rangle \tag{A8}$$

during that particular time interval. This result shows that exact tracking of $y_d^i(t)$ *will* be achieved during the interval it is monitored; however, it is necessary that $\langle\hat{O}_i(t_i)\rangle$ be equal to its desired initial value $y_d^i(t_i)$. Due to dynamical coupling this will likely not be the case, and therefore the objective trajectory itself may need to be corrected in order to match initial conditions.

The weights $w_j(t)$ could, in principle, be chosen arbitrarily, but here we seek a choice that will allow control over each $\hat{O}_j$, $j=1,\ldots,N$ as best as possible. One interesting possibility to achieve multioperator tracking is the stroboscopic case, where the weights $w_j(t)$ are periodic and are constructed such that while one strobe is "on" [i.e., $w_i(t)\approx 1.0$] the other strobes are "off" [i.e., $w_j(t)\approx 0.0$, $j\neq i$]. For example, if we consider a linear triatomic molecule where the objective trajectories are prescribe for both bonds $\langle\hat{r}_1\rangle_t$ and $\langle\hat{r}_2\rangle_t$, a suitable choice for the weights might be $w_1(t)=\sin^2(\omega_{\text{strobe}}t)$, $w_2(t)=\cos^2(\omega_{\text{strobe}}t)$.

In general, the degree to which each mode can be tracked optimally will depend on the physical nature of the problem. For example, the difficulty of the problem will increase as coupling between oscillators increases. Also, tracking of individual modes can be hampered if the individual modes have overlapping frequency structure. These aspects should be taken into account when choosing the value of strobe frequency ω_{strobe}, which will undoubtedly influence the controllability of the individual modes as well as the strength of the control field. Further analysis and numerical illustrations need to be performed to fully understand this method and to determine a strategy for finding the "optimal" strobing functions.

*Present address: Department of Chemistry, Panjab University, Chandigahr 160 014 India.

[1] D. J. Tannor and A. Rice, J. Chem. Phys. **83**, 5013 (1985); S. A. Rice, D. J. Tannor, and R. Kosloff, J. Chem. Soc. Faraday Trans. 2 **82**, 2423 (1986); P. Brumer and M. Shapiro, Acc. Chem. Res. **22**, 407 (1989).

[2] S. Shi, A. Woody, and H. Rabitz, J. Chem. Phys. **88**, 6870 (1988).

[3] P. Gross, D. Neuhauser, and H. Rabitz, J. Chem. Phys. **94**, 1158 (1991).

[4] A. P. Pierce, M. A. Daleh, and H. Rabitz, Phys. Rev. A **37**, 4950 (1988).

[5] A. E. Bryson and Y. Ho, *Applied Optimal Control* (Hemisphere, New York, 1975).

[6] A. Isidori, *Nonlinear Control Systems* (Springer-Verlag, New York, 1989)

[7] C. K. Ong, G. M. Huang, T. J. Tarn, and J. W. Clark, Math. Systems Theory **17**, 335 (1984).

[8] J. W. Clark, C. K. Ong, T. J Tarn, and G. M. Huang, Math. Systems Theory **18**, 33 (1985).

[9] Y.Chen, H. Singh, P. Gross, K. Mease, and H. Rabitz (unpublished).

[10] A. Hübler, Helv. Phys. Acta **62**, 343 (1989); A. Hübler, R. Georgii, M. Kuchler, W. Stelzl, and E. Lüscher, *ibid.* **61**, 898 (1988); R. Shermer, A. Hübler, and N. Packard, Phys. Rev. A **43**, 5642 (1991).

[11] A. Guldbergand and G. C. Billing, Chem. Phys. Lett. **186**, 229 (1991).

[12] M. D. Feit, J. A. Fleck, and A. Steiger, J. Comput. Phys. **47**, 412 (1982).

[13] R. Kosloff, J. Phys. Chem. **92**, 2087 (1988).

[14] A. Hübler, in *Modeling Complex Systems,* edited by L. Lam and V. Naroditsky (Springer-Verlag, New York, 1992).

[15] S. Chelkowski, A. D. Bandrauk, and P. B. Corkum, Phys. Rev. Lett. **65**, 2355 (1990).